Physicochemical characterizations of nanocellulose isolated from kudzu (Pueraria montana var. lobata) for potential packaging applications

Reid Love
Clemson University
Sneh Bangar
Clemson University
William S. Bridges
Clemson University
Duncan O. Darby
Clemson University
Hansol Doh
UC Davis: University of California Davis
William S. Whiteside (wwhtsd@clemson.edu)
Clemson University College of Agriculture Forestry and Life Sciences https://orcid.org/0000-0002-5958-8967

Research Article

Keywords: kudzu, cellulose nanocrystals, sustainable packaging, acid hydrolysis, nanocellulose

Posted Date: June 2nd, 2022

DOI: https://doi.org/10.21203/rs.3.rs-1650785/v1

Abstract

Flexible packaging is an integral part of the food supply chain due to its unique thermal, mechanical, and barrier properties. The many advantages (e.g., lightweight, product protection, reduction in food waste, communication medium, etc.) come with certain drawbacks (low recyclability rate, pollution of ecosystems, etc.). Still, the heavy reliance of the food industry on these products, many of them being unsustainable plastics derived from petrochemicals, is unlikely to diminish in the foreseeable future. Therefore, more sustainable alternatives that do not sacrifice performance (machinability, shelf-life, etc.) are needed before pollution becomes irreversible and public outcry insurmountable. Nanocellulose, especially in the form of cellulose nanocrystals (CNCs), can be incorporated into sustainable polymer matrices to enhance mechanical, thermal, and barrier properties. More research to find novel biomasses for CNC extraction would be welcomed by industry. One potential biomass source for the extraction of nanocellulose is the invasive deciduous perennial: kudzu (*peuraria montana* var. *lobata*). An industrial benefit for this agricultural nuisance may exist, however there has not been any formal research related to kudzu CNCs. The purpose of this research is to extract cellulose nanocrystals from kudzu and characterize them to evaluate their efficacy as an additive in degradable packaging solutions.

1. Introduction

The heavy reliance of the food industry on flexible packaging for its beneficial qualities is unlikely to diminish in the foreseeable future. In fact, a conservative model predicts that the production of plastic will increase by 10.8 million tons each year in the next decade (Brandon and Criddle 2019). This by far outstrips the estimated 0.8 million tons of plastic that are recycled each year in a time of increasing public dissent and decreasing landfill capacity. To combat this issue, many biopolymer-based plastics have been developed as alternatives to conventional petroleum-derived plastics in the packaging industry. However, performance, processing, and costs are the main hurdles that need to be addressed if these biopolymers are to replace conventional polymers on a large scale. For instance, the costs of biopolymers range from 3–10 times the price of conventional polyolefin plastics (Rodriquez-Perez et al. 2018). Biopolymers also struggle to meet the desired mechanical strength, thermal stability, molecular weight (MW) distribution, melt strength, and modulus needed for processing, as well as the barrier and water resistance required for consumer product protection (Lucas-Freile et al. 2018; Mensitieri et al. 2011; Petersen et al. 1999).

Biopolymer-based plastics may exhibit inadequate shelf-life performance, poor mechanical properties, and low thermal stability (Brandon and Criddle 2019). These limitations make food protection an issue, and they can be challenging to run on typical polymer processing, converting, and packaging equipment. The very properties that make a film compostable (such as structures that are subject to hydrolytic attack) often undermine its ability to be run efficiently on machinery such as blown, cast, extrusion, print, and package lines. Additionally, biopolymers generally have poor oxygen transmission rate (OTR) and water vapor transmission rate (WVTR) when compared to oil-derived plastics. Poor performance in these metrics negatively affects the shelf-life of some products. However, proven processes, such as the

addition of nucleating agents to increase crystallinity, can rectify some of these weaknesses. Therefore, more research must be conducted to generate sustainable nucleating agents that can be utilized as additives in sustainable packaging structures. Sustainable additives can thereby enhance the desired properties of the sustainable matrix while not taking away from the degradability of the composite.

A logical and cost-efficient sustainable additive would be the most abundant naturally occurring polymer on the planet, cellulose (Habibi et al. 2010). It is located in the cell walls of many biomasses (plants, bacteria, tunicates, etc.), making it a sustainable and renewable replacement of conventional polymers produced mainly from limited resources (Chakrabarty and Teramoto 2018; Yang et al. 2007). This biopolymer is available in various terrestrial and marine environments. In its native forms, cellulose exists in a matrix of largely composed of lignin and hemicellulose. To isolate cellulose, alkaline agents (e.g., caustic soda) and weak acids (e.g., acetic acid) have been used to solubilize and extract the non-cellulosic parts (Doh et al. 2020). However, these reactants will not reduce cellulose down to the mechanically superior cellulose nanocrystal (CNC), which has many advantages in the packaging industry due to high tensile strength (7.5–7.7 GPa) and elastic modulus (110–220 GPa with an average of around 170 GPa) while maintaining a low density (1.61 g/cm) (Habibi et al. 2010; Stark 2016). Furthermore, the high functionality of CNCs enables them to act as nucleating agents and increase the crystallinity of the surrounding polymer (Habibi et al. 2010). Thus, to fully leverage the mechanical strength of the cellulose molecule, amorphous factions of cellulose and non-cellulosic material must be discarded to isolate the highly crystalline and mechanically useful CNC.

The primary methods used to produce CNCs are enzymatic and acid hydrolysis. Following depolymerization and bleaching steps to remove non-cellulosic materials, this research will utilize acid hydrolysis to produce CNCs. The general process is illustrated in Fig. 1. During acid hydrolysis, the hydronium ion, produced by the hydrolyzing sulfuric acid, transversely breaks the glycosidic bonds of the accessible amorphous regions (Mozdyniewicz et al. 2016). Theoretically, the glycosidic break leaves the tightly packed crystalline micelle domain intact and substitutes sulfate esters throughout the CNCs (Khalil et al. 2015). These negatively charged sulfate groups are critical in minimizing aggregation (via repulsion forces) and forming stable solutions (Doh et al. 2020; Habibi et al. 2010; Wang et al. 2018). Sulfuric acid hydrolyzed CNCs self-assemble into a chiral nematic ordered phase in film and solvent suspensions (Habibi et al. 2010). The chiral nematic order of CNCs can be leveraged to design specific optical characteristics. Implementations of CNCs into a matrix can increase optical clarity up to a critical concentration (Chakrabarty and Teramoto 2018). However, being a hydrophilic non-thermoplastic polymer that tends to agglomerate, it is intrinsically difficult to extrude CNCs when compounded with the typical polymers in the sustainable packaging industry. Issues have included the molten curtain frequently breaking, the CNCs thermally degrading, and the CNCs significantly agglomerating during processing (Oksman et al. 2016). So, although it has gained academic notoriety (where small-scale solvent casting is the preferred method), it has yet to be widely adopted in large-scale industrial processes (Oksman et al. 2016). Nevertheless, sulfated nanocrystals have shown to decrease agglomeration, and recent advances in continuous melt processing such as co-rotating twin-screw extrusion, solid-state pulverization, grafting, and chemical pretreatment are making up for compounding

deficiencies (Oksman et al. 2016; Stark 2016). Thus, the two main issues in obtaining useful CNC composites are (1) removing non-cellulosic material from the biomass and amorphous factions from the native cellulose and (2) dispersing the CNCs throughout a matrix without significant agglomeration during processing.

This research will utilize kudzu (*Peuraria montana* var. *lobata)* as the biomass for CNC extraction. Kudzu, infamously known in the southeastern United States as “the vine that ate the South,” is an invasive species in the United States that overtakes and strangles surrounding due to its rapid growth (Gulizia and Downs 2019; Keung 2002). In its native environments (China, Japan, and other parts of Asia), the rapidly growing vine is kept at bay by numerous evolutionary counterforces. However, since kudzu has only been in the United States since the late 19th century, the vine is free to spread rapidly without much competition. It is a suffocating, semi-woody vine that is a strong climber that overtakes surrounding vegetation and man-made structures to achieve maximum photosynthesis. The vine exhibits diameters between 1-2.5 cm (Keung 2002). Three to five vines originate from a crown that sits in the topsoil connected underneath by bulbous and tubular-shaped roots that form a sizeable horizontal network one to three meters below the ground (Shurtleff and Aoyagi 1977). These large starchy roots (2–18 cm in diameter) contain an abundant energy reservoir that makes it a drought-resistant and fast-spreading plant in the warm months. The roots also firmly entrench the legume into the surrounding soil (Keung 2002; Shurtleff and Aoyagi 1977). The deeply entrenched roots and drought-resistant nature of kudzu make it a good candidate for preventing soil erosion. Nevertheless, the properties that make kudzu such a hardy plant also come with the trade-off of being extremely hard to exterminate and control (Keung 2002; Shurtleff and Aoyagi 1977). Given its exceptionally rapid propagation, it is now widely considered an agricultural nuisance. It is safe to say its removal and harvesting for alternative purposes would be welcomed by local populations in the United States. A newly found use for this noxious weed would significantly improve its perception, help regulate its proliferation, and provide a renewable resource to whichever industry can find it a value-added purpose (Luo et al. 2002).

This research believes that the packaging industry can use kudzu for CNC extraction. It is important to note that the properties of CNCs depend on the source, time of harvest, extraction methodology, mechanical treatment, chemical treatment, and scale of the cellulosic material (Khalil et al. 2015). Many studies have been conducted to determine the most effective source for nanocellulose extraction as shown in Table 1 (Chakrabarty and Teramoto 2018). Logically, higher cellulose compositions would lead to higher CNC yields. Furthermore, a higher aspect ratio is important when incorporating the CNCs into a polymer matrix to enhance mechanical, thermal, and barrier properties (Clyne and Hull 2019; Doh et al. 2020). Doh et al. (2020) demonstrated that two other plentiful but problematic species, the *Sargassum natans* (also known as sargassum seaweed) and *Laminaria japonica* (also known as kombu seaweed), produce CNCs with treatment and enhanced the mechanical and thermal properties of the composite. The sargassum seaweed contains approximately 20% cellulose, and the kombu seaweed contains 17% cellulose (Rabemanolontsoa and Saka 2013; Shi et al. 2011). Hence, even relatively low cellulose comprising sources can produce useful CNCs. Cellulose makes up 33% of the kudzu vine composition (Anele et al. 2020; Luo et al. 2002; Tanner et al. 1979; Wilke and Rosenberg 1977). The rest of the vine is

composed of hemicellulose (11%), lignin (14%), solubles (41.4%), and ash (0.3%) (Luo et al. 2002; Tanner et al. 1993). However, the kudzu aerial parts (leaf and stem) contain less cellulose (14–20%), less lignin (4–6%), and more hemicellulose (10–20%) on average when compared to the vine (Anele et al. 2020; Gulizia and Downs 2019). The composition percentages is highly dependent on if the kudzu was harvested in the early or late season (Gulizia and Downs 2019; Uludag et al. 1996). Furthermore, the cellulose of kudzu has been reported to have a relatively high complex viscosity and a high degree of polymerization (DP) above 1720 (Harland 1952; Li 2003). With sufficient acid concentration, the DP will reach a level-off degree of polymerization (LODP) independent of the source's initial DP before hydrolysis (Mozdyniewicz et al. 2016; Hamad and Hu 2010). Moreover, Hamad and Hu also show that crystallinity reaches a maximum of 90% around the LODP, and the nanocrystal reaches a minimum diameter of 8–10 nm, independent of the initial DP (Mozdyniewicz et al. 2016). Thus, kudzu, given its relatively high concentration of cellulose and its large DP, may present a viable biomass for the extraction of CNCs with relatively high aspect ratios.

1.5. Research Purpose

Due to the growing interest in biopolymers, the purpose of this research is to determine the efficacy of extracting nanocellulose from kudzu, characterize said nanocellulose, and compare it with extracted nanocellulose from other sources, such as seaweed biomass (Doh et al. 2020). The potential industrial consumption of a predominantly troublesome and invasive species clearly has its inherent advantages, especially with its target use being the growing sustainable packaging market. Numerous biomasses (cotton, hemp, flax, spruce, bamboo, seaweed, etc.) used acid hydrolysis to extract nanocellulose with varying degrees of concentration, time, temperature, and type of acid (Bondeson et al. 2006; Brito et al. 2012; Chen et al. 2016; Doh et al. 2020; Donaghy et al. 1990; Dong et al. 1998; Hamad and Hu 2010; Lu and Hsieh 2010; Luzi et al. 2014; Mondragon et al. 2014). However, according to the literature review of this field, the process to isolate nanocellulose from kudzu has never been documented, and consequently, its resulting characteristics have yet to be formally studied. Thus, the first objective of this research is to evaluate the effectiveness of previous isolation methods on two parts of kudzu biomass: the aerial and vine regions. The second objective is to characterize the resulting isolated nanocellulose particles and compare to previous sources of nanocellulose extraction to discern if the kudzu nanocellulose can provide any value to the sustainable packaging landscape

Table 1
Compositions of previous used sources for CNC extraction and their resulting aspect ratios ([1] Anele et al. 2020; [2] Doh et al. 2020; [3] Filson et al. 2009; [4] Gulizia and Downs 2019; [5] Khalil et al. 2015; [6] Lou et al. 2002; [7] Luzi et al. 2016; [8] Rabemanolontsoa and Saka 2013; [9] Shi et al. 2011; [10] Sundarraj and Ranganathan 2018; [11] Tanner et al. 1979; [12] Wilke and Rosenberg 1977).

Source	Composition (%)			Aspect Ratio (L/D)	References
	Cellulose	Hemicellulose	Lignin		
Cotton	95	2	1	10	5, 10
Flax (retted)	71	21	2	-	5, 10
Flax (unretted)	63	12	3	15	5, 10
Hemp	70	22	6	35	5, 7, 10
Kombu	17	31	0	11	2, 9
Kudzu (aerial)	14–20	10–20	4–6	?	1, 4
Kudzu (vine)	33	11	14	?	1, 6, 11, 12
Recycled Pulp	98	1	1	3–23	3
Sargassum	20	43	8	6	2, 8
Sisal	73	14	11	60	5, 10
Sugarcane Bagasse	40	30	20	64	5, 10
Wheat straw	30	50	15	45	5. 10
Wood	40–47	25–35	16–31	50	5, 10

2. Materials And Methods

2.1. Kudzu collection and preparation

Kudzu (*Pueraria montana* var. *lobata)* was harvested in late August. Both the aerial part (leaf/stem) and the vine were collected from a heavily infested area in Clemson, South Carolina, USA (34° 40’ 16.6” N, 82° 49’ 47.3” W). The aerial parts were washed with running tap water and then dried at 30ºC for 7 days in a laboratory drying oven. The aerial parts were then pulverized for 5 minutes using a commercial blender (Magic Bullet, USA) to produce a fine powder and then set aside to undergo chemical treatment.

The kudzu vine underwent a retting process like that of the Uludag et al. study (1996). This process utilized the enzymes naturally produced by the bacteria found in the kudzu vine to degrade the outer sheath and expose the fiber bundles (Uludag et al. 1996).The vines were approximately 1 cm in diameter and cut to lengths of 15 cm to be placed in a container of distilled water to soak. The soaking time was

determined to be the time needed for the measured pH (Orion Star™ A214 pH/ISE meter, Thermo Fisher Scientific, Massachusetts, USA) to decrease to a constant level of pH 5.5 (Uludag et al. 1996). This period was approximately 3–5 days. After retting, the outer sheaths were peeled off under running tap water. The fiber bundles were then isolated and dried for 24 hours at 30ºC. Finally, the fibers were pulverized using a commercial blender and put back in the oven for 72 hours at 30ºC.

2.2. Isolating nanocellulose from kudzu

After the leaf and vine powders were dried, the samples were subjected to a four-step treatment (depolymerization, bleaching, acid hydrolysis, and mechanical dispersion). Due to this study being the first known attempt to isolate nanocellulose from kudzu, the procedure was largely adapted from previous methods (Doh et al. 2020; Feng et al. 2015; Huq et al. 2012; Liu et al. 2017; Sung et al. 2017). All chemicals used were of analytical grade.

To begin the depolymerization step, the pulverized powders from the aerial part and vine were separately placed in two hydrochloric acid (HCl) solutions (0.2 M) at 1:15 proportion (w/v) and magnetically stirred for 2 hours at 30ºC. The colloidal suspensions were then washed with distilled water by centrifugation cycles (Avanti® 144 JXN-30, Beckman Coulter, Inc., Indiana, USA) at 15,000 *g* for 10 minutes to remove the supernatant. Once neutral pH was obtained, the residues of both the aerial part and vine were separately placed in distilled water at a 1:60 proportion (w/v). Then 4% sodium hydroxide (NaOH) was added to the solutions until the pH of the solutions were adjusted to approximately pH 10. These solutions were immediately placed on a hot-plate magnetic stirrer to continuously mix and heat the colloidal suspensions for 3 hours at 75ºC. After completion, the suspensions were washed by several centrifugation cycles at 15,000 *g* for 10 minutes to remove excess NaOH and isolate the remaining residues. Finally, the residues were placed in the laboratory oven to dry for 72 hours at approximately 65ºC.

The bleaching step was conducted by treating the polysaccharide residues with 10% potassium hydroxide (KOH), using a 1:20 solid to liquid ratio, for 3 hours at 30ºC. After this treatment, the residues from the aerial parts were set aside, and further treatment was aborted due to the minuscule amount of yield following this step. However, the treatment of the vine residue was continued. After washing with distilled water, the vine residue was treated for 12 hours with 6.5% (w/v) sodium hypochlorite (NaClO) at room temperature. The solution was then washed with distilled water by several cycles of centrifuging the samples at 15,000 g for 10 minutes. Then the pH was adjusted to pH 5 by gradual addition of glacial acetic acid (CH_3COOH). Once the desired pH was reached, the solution was stirred for 2 hours at room temperature. This step further removed the remaining hemicellulose by hydrolysis of glycosidic linkages and some of the lasting lignin by catalyzing the β-O-4 ether bonds (Sun et al. 2005; Tarasov et al. 2018). The second round of bleaching was conducted using 30% hydrogen peroxide (H_2O_2) (g/5 mL solid to liquid) for 70 minutes at 80ºC to further ensure the removal of lignin and any remaining hemicellulose (Chen et al. 2016). The solution was washed with distilled water and centrifuged (15,000 g for 10

minutes) for several cycles to remove the supernatant. The extracted bleached residue was then ready for acid hydrolysis.

During the acid hydrolysis step, the bleached residue was converted to nanocellulose by removing amorphous regions using 51% sulfuric acid (H_2SO_4). The residue was stirred in a beaker with 51% H_2SO_4 for 30 minutes at 45ºC with a 1:15 solid to liquid ratio. The solution was then washed with distilled water centrifuged at 15,000 g for several cycles to obtain a nanocellulose suspension with a pH close to that of distilled water. The pH of this suspension was then adjusted to approximately pH 7 with 4% NaOH. Finally, the colloidal suspension was mechanically dispersed using an ultrasonicator (Q700 Sonicator, Qsonica L.L.C., Connecticut, USA) at 30% amplitude for 15 minutes. The suspension was then immediately lyophilized by a commercial freeze dryer (Harvest Right™ Medium Freeze Dryer, Harvest Right™, Utah, USA) to prevent aggregation of the nanocellulose and yield a fine powder.

2.3. Characterization of CNCs from kudzu

2.3.1. Morphology analysis

The morphology of the nanocellulose sample was characterized using transmission electron microscopy (TEM, H-9500, Hitachi, USA). The nanocellulose samples were diluted with distilled water at 0.2–0.5% (w/v) for transmission electron microscope (TEM) sample preparation. The suspension was sonicated for 5 minutes, and then a drop was placed onto a SiO-based grid and allowed to dry overnight. The high-resolution TEM imaged the sample grids at an accelerating voltage of 300 kV. The dimensions (length and width) of the imaged nanocellulose samples were calculated using the ImageJ software (National Institute of Health, Bethesda, MD, USA). Ten different crystals in the image were measured for length (L) and diameter (D) to calculate the average aspect ratio (L/D) of the sample.

2.3.2. Fourier transform infrared spectrometry (FTIR) analysis

The untreated, bleached, and acid hydrolyzed vine underwent separate FTIR analyses. A milligram of each sample was individually placed on the crystal beam of the FTIR spectrometer (Nicolet iS10, Thermo Fisher Scientific, USA). Using the attenuated total reflectance (ATR) technique, each sample underwent 128 scans in the infrared wavenumber range of 500–4000 cm^{-1} with a resolution of 4 cm^{-1}.

2.3.3. X-ray diffraction (XRD) analysis

Samples also underwent X-ray diffraction (XRD) using the Rigaku Ultima IV X-ray diffractometer (Tokyo, Japan) to determine the crystallinity index (CI). The untreated, bleached, and acid hydrolyzed samples all underwent XRD analysis. Using a scanning ratio of 2 degrees/min and a range of 5–40 degrees, the samples were radiated with copper K-α (wavelength = 1.5418 Å) using a voltage of 40 kV and a current of 40 mA. The Segal method was used to determine the crystallinity and was calculated as follows:

$$\text{Crystallinity Index } (\%) = \frac{I_{200} - I_{am}}{I_{200}} \times 100$$

where I_{200} is the peak intensity of the (002) plane (2θ ≅ 23°C), and I_{am} is the peak intensity of the amorphous fraction (2θ ≅ 19°C) (Segal et al. 1959).

2.3.4. Thermogravimetric analysis

Different samples from the two treatment groups were analyzed with thermogravimetric analysis (TGA) (Hi-Res TGA Model 2950, TA, USA). The untreated vine sample, bleached vine sample, and acid hydrolyzed sample all underwent TGA analysis. The samples were tested by placing 2–10 mg on an aluminum pan in the device which was burned under a nitrogen gas atmosphere. The heating cycle was from 30°C to 600°C with a ramp rate of 10°C/min. Derivative thermogravimetric (DTG) data was also generated from the TGA analysis to better understand each treatment group's heat degradation profile. The DTG data were calculated using the following formula:

$$\text{Derivative Weight } \left(\frac{\%\ \text{weight change}}{\text{min}}\right) = -\frac{\frac{m_i - m_{i-1}}{m_o} \times 100}{t_i - t_{i-1}}$$

where m_i is the mass of the sample at the ith index, t_i is the time (in minutes) at the ith index, and m_o is the mass of the original sample before heating. The data were corrected for noise using an exponential smoothing software package.

2.4. Statistical analysis

Most results in this study are descriptive, so the statistical analysis was only used to compare the dimensions of the nanocellulose obtained in this study versus the dimension of nanocellulose from previous studies. For instance, the average aspect ratio, length, and diameter of the extracted kudzu nanocellulose were compared to that of the Doh et al. (2020) study that extracted seaweed nanocellulose. Analysis of means using a *t*-test (as well as a Wilcoxon signed-rank test where appropriate) was used to determine any statistically significant difference between the aspect ratios, lengths, and diameters of the respective nanocellulose extractions ($p \leq 0.05$).

3. Results And Discussion

Nanocellulose samples were obtained by treating the vine under the described procedure. However, the yield of the kudzu leaf after the depolymerization was too low to continue with further treatment. Although the leaf is a good source of fodder due to its high crude protein content, it has a lower amount of cellulose (14–20%) compared to the vine (33%), as shown in Table 2 (Anele et al. 2020; Gulizia and

Downs 2019; Tanner et al. 1993). Furthermore, the leaf's comparatively low acid detergent fiber resulted in significant degradation during acid treatment to be efficiently utilized in this study (Anele et al. 2020; Gulizia and Downs 2019; Tanner et al. 1993). Therefore, only the samples produced from the vine were analyzed, and the results are discussed below.

3.1. Morphology analysis

The TEM image in Fig. 2 clearly reveals that the kudzu vine was isolated into its cellulose nanocrystal (CNC) form upon treatment. The microscope used a resolution in the nanoscale range, and thus the rod-shaped particles indicated that the sample did in fact contain CNCs. Furthermore, CNCs are defined as having an aspect ratio between the range of 1-100, and the results in Table 2 exhibited an average aspect ratio of 6.43 ± 1.78 for the kudzu vine sample (Doh et al. 2020). Thus, the particles shown in the sample were within the CNC aspect ratio range. When compared to the Doh et al. (2020) samples (who used a similar procedure), the average aspect ratio of the kudzu vine CNCs (Table 2) was equivalent to the sargassum seaweed (no statistical significance found) but smaller than that of the kombu seaweed (statistical significance found). The significantly higher length of the kudzu vine CNCs as compared to the seaweed CNCs could be attributed to the cellulose contained in kudzu having a high DP (Li 2003; Vanderfleet and Cranston 2021). However, the lower average aspect ratio of kudzu CNCs (6.43 ± 1.78) relative to the kombu seaweed CNCs (11.13 ± 1.84) was a product of the larger diameter of the kudzu vine CNCs (statistical significance found). A reasonable explanation for the larger diameter could be the lower hemicellulose content in the kudzu vine as compared to seaweed sources. This is in accordance with previous studies. Mozdyniewicz et al. (2016) reported a higher fibril width with decreasing hemicellulose content. Duchesne et al. (2001) explained that the lower hemicellulose content allowed the cellulose fibrils to aggregate and recrystallize upon treatment, thereby forming a larger structure.

Table 2
The dimensions (length, diameter, and aspect ratio) of the imaged kudzu vine CNCs measured and statistically analyzed versus the Doh et al. seaweed CNCs (Doh et al. 2020).

Source	Length[1,2] (L) (nm)	Diameter[1,2] (D) (nm)	Aspect Ratio[1,2] (unitless)
Kudzu Vine	285.01 ± 150.33[a]	42.78 ± 13.26[a]	6.43 ± 1.78[a]
Sargassum (Doh et al. 2020)	49.30 ± 11.73[b]	8.55 ± 2.11[b]	6.11 ± 1.85[a]
Kombu (Doh et al. 2020)	228.14 ± 46.07[c]	20.96 ± 5.11[c]	11.13 ± 1.84[b]
(1) Data are mean ± S.D.			
(2) Values with different superscripted letters within a column denote that there was statistical significance found by *t*-test ($p \leq 0.05$).			

3.2. FTIR Analysis

The FTIR data from the untreated vine, bleached vine, and acid hydrolyzed vine were analyzed to gain insight into the chemical structure changes of the samples. As a general trend, the bleached vine and acid hydrolyzed vine spectra differed from the untreated vine sample in some key wavenumber bands, as shown in Fig. 3. These distinct differences showed that the lignin, hemicellulose, and other non-cellulosic materials were removed with the performed treatment. The untreated vine sample showed three peaks specific to the presence of lignin and hemicellulose that were reduced in the bleached vine spectra and were non-existent in the acid hydrolyzed vine spectra. First, the peak at 1236 cm^{-1} in the untreated vine sample, which is characteristic of the aryl-alkyl ether linkages in lignin, disappeared in the bleached vine and acid hydrolyzed samples, demonstrating the elimination of lignin in these treated samples (Morán et al. 2008). Second, the untreated vine sample exhibited a band in the 1500–1600 cm^{-1} range, which indicated the presence of lignin aromatic rings. This band was not observed in the bleached and acid hydrolyzed samples. The band at 1507 cm^{-1} indicates the vibrating aromatic rings, and hence the absence of any band in this range demonstrated the removal of lignin with treatment (Luzi et al. 2014; Morán et al. 2008). Lastly, the untreated vine exhibited a pronounced peak at 1733 cm^{-1}, whereas the bleached vine showed it to a much less extent, and the acid hydrolyzed registered no peak at this wavenumber. This could be attributed to the atomic vibrations of several groups present in hemicellulose and lignin: (1) the acetic and uronic acid ester groups unique to hemicellulose, or (2) the carboxylic acid ester groups in ferulic and *p*-coumaric acids characteristic to both lignin and hemicellulose (Alemdar and Sain 2008; Chandra et al. 2016; Chirayil et al. 2014; Sun et al. 2005). The removal of these peaks

furthermore demonstrated the isolation of cellulose from the surrounding hemicellulose and lignin components in the cell wall matrix via the performed treatments.

The FTIR data also provides insights into the cellulose structure of the samples. In Fig. 3(b), the peak around 896 cm^{-1} was associated with the deformation of the β-glycosidic C-H linkages of cellulose (Alvarez and Vázquez 2006; Chirayil et al. 2014; Luzi et al. 2014; Oh et al. 2005). As the treatment increased, this peak became more pronounced. A broad band with a relative strong intensity indicated cellulose I structure, whereas a weak intensity was associated with relatively amorphous cellulose (Nelson & O'Connor 1964) The bleached vine and acid hydrolyzed samples demonstrated a more crystalline structure based on this peak intensity compared to the untreated vine sample. Furthermore, peaks between 1105–1110 cm^{-1} are hallmark bands of the cellulose I structure (Chen et al. 2016). The peak at 1105 cm^{-1} shifted to 1109 cm^{-1} after the acid hydrolysis, which signaled the cellulose I structure (Chen et al. 2016; Nelson & O'Connor 1964). On the other hand, the subdued shoulder for the untreated vine sample in this region further indicated the relative amorphousness of this sample compared to that of the treated samples. Similarly, a shift from 1424 cm^{-1} (untreated sample) to 1428 cm^{-1} (treated samples) was representative of C-H_2 scissoring motion, where a strong 1428 cm^{-1} peak indicated cellulose I and a less intense peak around ~ 1420 cm^{-1} suggested a decrease in crystallinity (Nelson & O'Connor 1964). For the treated samples, the band at 1161 cm^{-1} was associated with the C-O-C stretching of the antisymmetric glycosidic linkages in cellulose I (Liang and Marchessault 1959). This band was shifted to 1155 cm^{-1} in the untreated vine sample, indicating a more amorphous structure (Nelson & O'Connor 1964). Compared to the weak 1155 cm^{-1} peak for the untreated sample, the increased intensity of the 1161 cm^{-1} peaks of the treated samples could be explained by the removal of lignin and hemicellulose (Chandra et al. 2016; Chen et al. 2016; Marchessault and Liang 1962). As the lignin and hemicellulose were removed, the treated samples were allowed to fall into more compact and crystalline structures relative to the more heterogeneously structured, untreated sample. Additionally, the peaks in the 1047–1055 cm^{-1} range further demonstrate the isolation of cellulose in the treated samples. This range corresponded to the pyranose structure of cellulose, and its increasing intensity with treatment pointed to the increasing content of cellulose and decreasing content of non-cellulosic components (Doh et al. 2020; Sun et al. 2005; Yahya et al. 2015). To the right of this range is the 1032 cm^{-1} band, which showed the vibrations of the C-O stretching in cellulose and was most pronounced in the acid hydrolyzed vine sample (Zhuang et al. 2020). This increased intensity further demonstrated the enhanced isolation of cellulose with the hydrolysis treatment. However, it is essential to note that spectra of cellulose, lignin, and hemicellulose overlap at specific regions, so caution should be taken in reporting conclusive results. The region around the 1032 cm^{-1} wavenumber is one area of overlap. As previously stated, it could indicate C-O stretching in cellulose, but this band is also simultaneously characteristic of C-H in-plane deformations found in lignin (Zhuang et al. 2020). Consequently, the possibility of residual lignin in bleached and acid hydrolyzed vine samples could not be eliminated via FTIR analysis.

The bands associated with bound water and hydrogen bonding also helped distinguish the degree of crystallinity in the samples. It is advantageous for most packaging materials to be as hydrophobic as possible. The broad peaks in the 1603–1640 cm^{-1} provides insight into relative amount of water entrapped in the structure via hydrogen bonding (Chandra et al. 2016; Chen et al. 2016; Chirayil et al. 2014; Oh et al. 2005). As shown in Fig. 3(a), the peak intensity for the range was higher for the raw sample. Hence, there were fewer carboxylate groups and bound water molecules in the bleached vine and acid hydrolyzed vine samples, making them more ideal candidates for packaging materials (Chirayil et al. 2014; Nacos et al. 2006).

Furthermore, key bands in the 1316–1370 cm^{-1}, 2900 cm^{-1}, and 3300–3400 cm^{-1} regions (Fig. 3(b)) are linked to the degree of hydrogen bonding (Doh et al. 2020). The 1368–1370 cm^{-1} peaks indicated the symmetric stretching of the C-OH bonds, whereas the 1316–1317 cm^{-1} indicated the asymmetric C-H deformations, and the 1335 cm^{-1} peak demonstrated the O-H bending in crystalline cellulose (Chen et al. 2016; Higgins et al. 1961; Luzi et al. 2014). The decrease in intensity or absence of these bands in the untreated vine spectra pointed to a lower degree of hydrogen bonding. Thus, it can be concluded that hydrogen bonding was increased in the treated samples, and thus a more crystalline structure was formed in these samples (Nelson & O'Connor 1964). To further expand on this point, the peaks at ~ 2900 cm^{-1} in Fig. 3(a) became progressively more intense and acute from the untreated sample to the treated samples. These bands were associated with the C-H stretching vibrations present in the cellulose rings as the degree of hydrogen bonding increased both inter and intramolecularly (Oh et al. 2005). The broad peak centered around 3300 cm^{-1} has historically been sensitive to the extent and type of hydrogen bonding present (Alvarez and Vázquez 2006; Chandra et al. 2014; Chirayil et al. 2014; Oh et al. 2005). Hence, the higher the wavenumber in this 3300–3400 cm^{-1} range corresponded to more intramolecular hydrogen bonding occurring between the O3-H and the pyranose O5 (Oh et al. 2005). The lower the wavenumber, the more intermolecular hydrogen bonding occurs between O6-H and the O3 of the neighboring cellulose molecule.

The integrated areas under the peaks for the bleached vine sample and the acid hydrolyzed vine sample in this region were approximately equal, indicating similar degrees of crystallinity. This finding was corroborated by XRD analysis (Fig. 4). Moreover, the area under the curve for the untreated sample was significantly lower, and thus it was expected to have a more amorphous nature relative to the treated samples. Thus, the FTIR results demonstrated that the treatments did remove non-cellulosic parts from the raw vine, however, in terms of determining CI, more conclusive evidence was collected via XRD analysis.

3.3. XRD analysis

The XRD results are shown in Fig. 4, and the calculated crystallinity indexes (by the Segal method) are reported in Table 3. Previous studies reported that the cellulose I structure will demonstrate peaks when 2θ is approximately 15–16 degrees, 22–23 degrees, and 34–35 degrees (Chirayil et al. 2014; Doh et al.

2020; Luzi et al. 2014; Mandal and Chakrabarty 2011; Sung et al. 2017). Peaks at 2θ = 22–23° are characteristic of the distance between the stacked sheets of adjacent cellulose chains that are held tightly together by hydrogen bonding (Luzi et al 2014). The 2θ = 15–16° and 2θ = 34–35° peaks are indicative of the orientation of chains along the fiber length (Luzi et al. 2014). Observed pronounced peaks with treatment (Fig. 4) demonstrated that the treatment successfully isolated cellulose I. These findings agree with the previously reported FTIR results. It is interesting to note that the bleached vine sample and the acid hydrolyzed sample were essentially equal in crystallinity, as shown in the XRD patterns and the reported crystallinity indices. This might be due to the prolonged exposure to NaClO, which worked as a significant oxidizing agent, followed by the separate treatment with acetic acid, which worked as a significant hydrolyzing agent, combining to have a strong oxidization and subsequent hydrolytic effect. The acetic acid may have already begun to hydrolyze the easily accessible glycosidic bonds (made easier by the preceding oxidation step) of hemicellulose and amorphous cellulose even before sulfuric acid hydrolysis was reacted (Mozdyniewicz et al. 2016). This effect would also account for the slight decrease in CI from the bleached vine sample (90.8%) to the acid hydrolyzed sample (90.0%). If the amorphous factions were already degraded by acetic acid, then the sulfuric acid would only decrease particle size and crystallinity by chain scission of crystalline parts.

The results from Table 3 further support the claim made in the FTIR analysis that non-cellulosic and amorphous components were increasingly degraded in each progressive treatment step. This was especially apparent in the bleaching step, where it accounted for the approximately 11.4% increase in CI upon treatment. This increase in CI with treatment was confirmed by previous studies (Mandal and Chakrabarty 2011; Sung et al. 2017). Moreover, the 90.0% CI of the acid hydrolyzed vine was higher than the sargassum seaweed CI (85.1%) and higher than the reported CI of pure cellulose samples (41.4–60%) (Doh et al. 2020; Sung et al. 2017). However, the CI for acid hydrolyzed kudzu vine was not as high as the impressive CI of the kombu seaweed CNCs (98.9%) isolated by Doh et al. (2020) using similar methods. Nevertheless, a CI of 90% was as close as some sources can reach to perfectly crystalline cellulose (Hamad and Hu 2010). It was above the 80% benchmark needed to self-assemble into a chiral nematic phase that offers enhanced optical and mechanical properties (Hamad and Hu 2010). In fact, purely crystalline CNCs may be disadvantageous in packaging applications since some degree of amorphousness is beneficial in selecting for certain viscoelastic and rheological behaviors (Hamad and Hu 2010).

Table 3
The calculated crystallinity indexes (using Segal method) of the kudzu vine after different stages of treatment compared to the Doh et al. (2020) seaweed samples (Segal et al. 1959).

Sample [Reference]	Crystallinity Index (%)
Untreated Vine	79.4
Bleached Vine	90.8
Acid Hydrolyzed Vine	90.0
Sargassum Seaweed [9]	85.1
Kombu Seaweed [9]	98.9

3.4. Thermal Analysis

The thermal degradation profiles of samples after different treatments are shown in Fig. 5. All samples demonstrated some weight loss in the range from 25–125°C which can largely be attributed to the evaporation of bound water (Doh et al. 2020; Mondragon et al. 2014). However, some samples indicated more weight loss than others. This can be explained by the presence of less lignin as treatment increases from untreated vine to acid hydrolyzed vine. The amorphous lignin envelopes the more crystalline cellulose in the plant cell wall and acts as a barrier that helps cellulose retain its bound water (Khalil et al. 2015). Upon removal of the lignin with successive treatment, the cellulose retained less water, and the water attached to the hydrophilic cellulose could be quickly evaporated. Thus, the acid hydrolyzed vine sample lost ~ 1.5% and the bleached vine sample lost ~ 4% of its weight in this range. Compare these to the weight loss of the untreated vine (~ 5.5%) in this 25–125°C region, and it can be determined that more extensive treatment results in less bound water. More treatment generally yields higher crystallinity, and the more crystalline samples were less likely to allow water to bind and become entrapped because of the more densely packed factions (Mondragon et al. 2014). However, the bleached vine sample (90.8% CI) had a higher weight loss than the acid hydrolyzed sample (90.0% CI). This may be attributed to higher contents of the characteristically water-entrapping lignin. Furthermore, the lower weight loss of the acid hydrolyzed sample as compared to the lesser treated samples could be explained by (1) the acid hydrolysis step was an intrinsically dehydrating mechanism, and (2) the presence of sulfate groups and acetyl groups in the remaining amorphous faction that replaced the hydroxyl groups of cellulose led to lower hydrogen bonding and overall higher hydrophobic character (Mandal and Chakrabarty 2011).

Hemicellulose largely decomposes exothermically in the 220–315°C range, and the maximum degradation of pure hemicellulose has been reported to occur around 260–270°C (Yang et al. 2007). As seen in Fig. 5(b), the untreated vine and bleached vine samples exhibited significant increases in derivative weight in this range. Although other lignocellulosic materials were degrading in this range, much of this increase could be attributed to hemicellulose. The depolymerization and bleaching process largely removed hemicellulose, but it is likely that some hemicellulose remnants remained in the bleached

sample accounting for the increased derivative weight (Fig. 5(b)) in this range. Yet, these remnants were largely dissolved and discarded during acid hydrolysis (Doh et al. 2020). Hence, acid hydrolyzed vine samples were much less affected around the max degradation temperature.

Pyrolysis of pectin exothermically occurred in a relatively wide range of 200–400°C (Mondragon et al. 2014). The bleaching process, specifically the treatment with KOH, is reported to be an efficacious way to remove non-cellulosic material while leaving much of the cellulose intact (Doh et al. 2020; Sung et al. 2017). As demonstrated in Fig. 5(a), the TGA curves of the bleached and acid hydrolyzed samples stayed above the curves of the untreated samples. This could be attributed to the increased presence of pectin in the depolymerized and untreated samples. The pectin in these samples would be burning off in the untreated sample, accounting for the increased weight change. The substantial DTG (Fig. 5(b)) increase around 180–220°C for the untreated vine and, to a lesser extent, the bleached vine is indicative of pectin and hemicellulose burning off at higher rates than the acid hydrolyzed vine samples. This lower DTG rate in the 180–220°C for the acid hydrolyzed vine could be explained by the trace amounts of hemicellulose and pectin after the bleaching step (Mondragon et al. 2014).

Due to its varied composition and aromatic structure, lignin has the broadest range of thermal degradation from 150–900°C (Yang et al. 2007). It decomposes exothermically until approximately 550°C, where it can then thermally degrade all the way to 900°C endothermically (Yang et al. 2007). Since lignin decomposes at such a wide range, it is difficult to determine the exact point of maximum degradation. However, samples with higher lignin concentration will exhibit a broader thermal degradation profile due to the difficulty of decomposing the aromatic rings and its diverse branches (Mandal and Chakrabarty 2011; Yang et al. 2007). This effect was observed in the broader DTG curves of the untreated vine and bleached vine samples relative to the narrow acid hydrolyzed sample (Fig. 5(b)). This finding relates to the crucial premise that the bleached sample may have contained more lignin than the acid hydrolyzed samples. In fact, the DTG curve of the bleached sample was approximately as broad as the DTG curve of the untreated vine, whereas the acid hydrolyzed vine sample exhibited a much narrower curve. This would suggest the significant presence of lignin in both the untreated vine and bleached vine samples relative to a small amount of lignin in the acid hydrolyzed sample. Even more, the DTG curve of the bleached vine sample exhibited a sharp increase in the 150–250°C range, where lignin would start to show a significant increase in degradation (Yang et al. 2007). Therefore, the bleached vine sample was far more likely to contain lignin relative to the acid hydrolyzed vine because most of the lignin was dissolved with sulfuric acid during the acid hydrolysis step.

Furthermore, cellulose is a less branched and more homogenous material than lignin, pectin, and hemicellulose, thereby making it stronger, denser, and more thermally stable (Yang et al. 2007). Therefore, the onset of thermal degradation will happen at a higher temperature. Yet, once degradation initiates in the cellulose, it will be in a narrower range due to the lack of impurities. This suggests that the presence of impurities (such as lignin, pectin, and hemicellulose) in the lesser treated samples contributed to a lower onset of thermal decomposition temperature since the non-cellulosic components lack the inherent

crystallinity of cellulose and provide more accessible active sites for thermal degradation (Doh et al. 2020; Lee et al 2018; Mandal & Chakrabarty 2011; Mondragon et al. 2014; Yang et al. 2007).

As alluded to in the previous paragraph, cellulose is reported to have the narrowest window of thermal degradation between 315–400°C (Yang et al. 2007). It also has a crucial distinction from the non-cellulosic components: it degrades endothermically at temperatures below 500°C (Yang et al. 2008). This can be attributed to different mechanisms during heating. Much of the cellulose mass will largely volatize (endothermically) into carbon monoxide (CO) and carbon dioxide (CO_2), whereas much of the mass in non-cellulosic components will largely char (exothermically) at temperatures below 500°C (Yang et al. 2008). However, the amount of residue appeared to have been larger in the acid hydrolyzed sample. This could be attributed to several (but not mutually exclusive) hypotheses. First, the more severely treated samples have higher crystallinity, thus making them more thermally stable (Doh et al. 2020; Mondragon et al. 2014). In addition, the more severely treated samples underwent more chemical reactions and were likely to have more molecules grafted onto the parent chain, such as acetyl groups, Na-cellulose formations, and sulfate groups (Mondragon et al. 2014). The sulfated groups of the acid hydrolyzed sample also gave the structure flame resistance, which could have also accounted for its low charring rate and larger residue after TGA analysis (Mandal and Chakrabarty 2011). In general, the presence of sulfate groups have been reported to hinder thermal stability in many facets: (1) sulfate groups act as initiators for thermal decomposition, (2) the negative charges and relative bulkiness of sulfate groups create more interchain space and thereby expose more of the nanocellulose surface area to the heat source, (3) acid hydrolysis with sulfuric acid not only attacks and cleaves the glycosidic bonds of the amorphous nanocellulose, but it penetrates into crystalline parts causing chain scission and lower molecular weight (Lu and Hsieh 2010; Mandal and Chakrabarty 2011; Mondragon et al. 2014). It is well understood that treating with sulfuric acid lowers thermal stability (Doh et al. 2020; Lu and Hsieh 2010; Mandal and Chakrabarty 2011; Mondragon et al. 2014).

The onset of thermal degradation of the acid hydrolyzed sample is lower than that of pure cellulose (Yang et al. 2007). One possible reason could be the increased thermal conductivity of nanocellulose (Shimazaki et al. 2007). This is achieved by the decrease in photon scattering of nanocellulose as compared to larger cellulose molecules which tend to have a less efficient photon pathway leading to poorer thermal conductivity (Shimazaki et al. 2007). The increase in thermal conductivity of the nanocellulose led to a more efficient and quicker thermal degradation relative to pure cellulose (Lu and Hsieh 2010; Yang et al. 2007). However, it was observed that with increased treatment, the onset temperature increased, and the DTG curve peaks moved to the right. Thus, it can be concluded that, although pure cellulose may be more thermally stable than these nanocrystals, the thermal stability was observed to increase with more treatment due to the removal of the amorphous non-cellulosic part. It is believed that increased thermal stability with treatment is due to the removal of amorphous parts allowing for the reorganization and tighter packing of crystalline cellulose factions.

4. Conclusions

Confirmed by the results of FTIR and TGA, non-cellulosic materials (lignin, hemicellulose, pectin, etc.) were observed to be solubilized and discarded from the kudzu vine via the depolymerization, bleaching, and acid hydrolysis step. The XRD results demonstrated a CI of 90.0% for the acid hydrolyzed CNCs. The bleached vine already exhibited a high CI (90.8%) before the acid hydrolysis step. However, upon further examination of its thermal properties, it appeared the acid hydrolysis is needed to remove remnants of lignin, increase the thermal stability, and protect against agglomeration via the repulsion effect of the acquired sulfate groups. On the other hand, the kudzu leaf is not an adequate biomass for CNC extraction, at least by means of this concentrated chemical treatment. A low concentration of HCl acid proved to be too intense for the kudzu leaf and quickly degraded the whatever present cellulosic component.

It can be concluded that the kudzu vine presents a novel source for nanocellulose extraction. TEM results confirmed that cellulose was present in its nanoform after treatment. The average aspect ratio was found to be 6.43 ± 1.78, which classifies as a cellulose nanocrystal (CNC). The average length of the CNCs was impressive (285.01 ± 150.33 nm) due to the large DP of kudzu cellulose. Yet, the large average diameter (42.78 ± 13.26 nm) decreased the average aspect ratio. It is thought that the relative lack of hemicellulose present in native kudzu compared to other sources creates a clustering effect of cellulose chains via intense hydrogen bonding between the hydroxyl groups of neighboring cellulose molecules. This causes an agglomeration of stacked chains and thus a larger average CNC diameter. However, the CNCs extracted from the sargassum seaweed in the Doh et al. (2020) study had an average aspect ratio smaller than 6.43 ± 1.78 (statistical significance found). Despite their small average aspect ratio, the sargassum seaweed CNCs still enhanced mechanical properties in a matrix. The comparable crystallinity and aspect ratio of the kudzu CNCs with respect to CNCs extracted from other biomasses, specifically the Doh et al. (2020) sargassum seaweed, points to its potential as a mechanically enhancing nanofiller in sustainable packaging polymers. It has the crystallinity needed to form self-assembled chiral nematic structures in a matrix and a sufficient aspect ratio to thereby enhance the mechanical and optical properties of the targeted polymer matrix. Future studies should aim to increase the aspect ratio by reducing the diameters of the kudzu CNCs. Adding treatment steps such as carding, high-pressure homogenization, and steam explosion (to name a few) may be able to disrupt the hydrogen bonding of the cellulose chains in the CNCs (decreasing the diameter) while not causing chain scission (thereby keeping the superb length).

Given that the subsequent acetic acid treatment yielded such a high CI, it may be beneficial in future studies to determine if higher concentrations (> 51%) of sulfuric acid would yield even greater CI. Future research should also incorporate these kudzu acid hydrolyzed CNCs into various sustainable matrices to study their impact as a nanofiller. Research is already underway to examine the mechanical, thermal, and barrier effects of implementing these specific kudzu CNCs into starch matrices. Increasing adhesion by grafting and blending the CNCs with synergetic polymers may be warranted to enhance composite performance. Finally, there remain some broader concerns from this area of research that are seldom discussed. As witnessed, the process to extract these “sustainable materials” requires the use of very hazardous chemicals, which have the potential for detrimental environmental impacts if utilized in high

volumes. If this process is to become more commercially prevalent, sustainable extraction methods need to be further developed, such as using enzymatic hydrolysis or steam explosion to produce CNCs.

Declarations

Acknowledgements

Declarations of interests: none.

Funding: This research did not receive any specific grant from funding agencies in the public, commercial, or not-for-profit sectors.

Funding

The authors declare that no funds, grants, or other support were received during the preparation of this manuscript.

Competing Interests

The authors have no relevant financial or non-financial interests to disclose.

Author Contributions

All authors contributed to the study conception and design. Material preparation, data collection and analysis were performed by Reid Love. The first draft of the manuscript was written by Reid Love and all authors commented on previous versions of the manuscript. All authors read and approved the final manuscript.

References

1. Alemdar A, Sain M (2008) Isolation and characterization of nanofibers from agricultural residues–Wheat straw and soy hulls. Bioresour Technol 99(6):1664–1671
2. Alvarez VA, Vázquez A (2006) Influence of fiber chemical modification procedure on the mechanical properties and water absorption of MaterBi-Y/sisal fiber composites. Compos Part A: Appl Sci Manufac 37(10):1672–1680
3. Anele UY, Anike FN, Davis-Mitchell A, Isikhuemhen OS (2020) Solid-state fermentation with Pleurotus ostreatus improves the nutritive value of corn stover-kudzu biomass. Folia Microbiologica, pp 1–8
4. Bondeson D, Mathew A, Oksman K (2006) Optimization of the isolation of nanocrystals from microcrystalline cellulose by acid hydrolysis. Cellulose 13(2):171–180
5. Brandon AM, Criddle CS (2019) Can biotechnology turn the tide on plastics? Curr Opin Biotechnol 57:160–166

6. Brito BS, Pereira FV, Putaux JL, Jean B (2012) Preparation, morphology and structure of cellulose nanocrystals from bamboo fibers. Cellulose 19(5):1527–1536
7. Chakrabarty A, Teramoto Y (2018) Recent advances in nanocellulose composites with polymers: a guide for choosing partners and how to incorporate them. Polymers 10(5):517
8. Chandra J, George N, Narayanankutty SK (2016) Isolation and characterization of cellulose nanofibrils from arecanut husk fibre. Carbohydr Polym 142:158–166
9. Chen YW, Lee HV, Juan JC, Phang SM (2016) Production of new cellulose nanomaterial from red algae marine biomass Gelidium elegans. Carbohydr Polym 151:1210–1219
10. Chirayil CJ, Joy J, Mathew L, Mozetic M, Koetz J, Thomas S (2014) Isolation and characterization of cellulose nanofibrils from Helicteres isora plant. Ind Crops Prod 59:27–34
11. Clyne TW, Hull D (2019) An introduction to composite materials. Cambridge university press
12. Doh H, Dunno KD, Whiteside WS (2020) Preparation of novel seaweed nanocomposite film from brown seaweeds Laminaria japonica and Sargassum natans. Food Hydrocolloids 105:105744
13. Donaghy JA, Levett PN, Haylock RW (1990) Changes in microbial populations during anaerobic flax retting. J Appl Bacteriol 69(5):634–641
14. Dong XM, Revol JF, Gray DG (1998) Effect of microcrystallite preparation conditions on the formation of colloid crystals of cellulose. Cellulose 5(1):19–32
15. Duchesne I, Hult E, Molin U, Daniel G, Iversen T, Lennholm H (2001) The influence of hemicellulose on fibril aggregation of kraft pulp fibres as revealed by FE-SEM and CP/MAS 13C-NMR. Cellulose 8(2):103–111
16. Feng X, Meng X, Zhao J, Miao M, Shi L, Zhang S, Fang J (2015) Extraction and preparation of cellulose nanocrystals from dealginate kelp residue: structures and morphological characterization. Cellulose 22(3):1763–1772
17. Filson PB, Dawson-Andoh BE, Schwegler-Berry D (2009) Enzymatic-mediated production of cellulose nanocrystals from recycled pulp. Green Chem 11(11):1808–1814
18. Gulizia JP, Downs KM (2019) A review of kudzu's use and characteristics as potential feedstock. Agriculture 9(10):220
19. Habibi Y, Lucia LA, Rojas OJ (2010) Cellulose nanocrystals: chemistry, self-assembly, and applications. Chem Rev 110(6):3479–3500
20. Hamad WY, Hu TQ (2010) Structure–process–yield interrelations in nanocrystalline cellulose extraction. Can J Chem Eng 88(3):392–402
21. Harland WG (1952) Relation between intrinsic viscosity and degree of polymerization. Nature 170(4329):667–667
22. Higgins HG, Stewart CM, Harrington KJ (1961) Infrared spectra of cellulose and related polysaccharides. J Polym Sci 51(155):59–84
23. Huq T, Salmieri S, Khan A, Khan RA, Le Tien C, Riedl B, Fraschini C, Bouchard J, Uribe-Calderon J, Kamal MR (2012) Nanocrystalline cellulose (NCC) reinforced alginate based biodegradable

nanocomposite film. Carbohydr Polym 90(4):1757–1763
24. Keung WM (ed) (2002) Pueraria: the genus Pueraria. CRC Press
25. Khalil HA, Bhat AH, Bakar AA, Tahir PM, Zaidul ISM, Jawaid M (2015) Cellulosic nanocomposites from natural fibers for medical applications: A review. Handbook of polymer nanocomposites.Processing, performance and application,475–511
26. Lee H, Sundaram J, Zhu L, Zhao Y, Mani S (2018) Improved thermal stability of cellulose nanofibrils using low-concentration alkaline pretreatment. Carbohydr Polym 181:506–513
27. Li Z (2003) Rheology of lyocell solutions from different cellulosic sources and development of regenerated cellulosic microfibers. The University of Tennessee
28. Liang CY, Marchessault RH (1959) Infrared spectra of crystalline polysaccharides. I. Hydrogen bonds in native celluloses. J Polym Sci 37(132):385–395
29. Liu Z, Li X, Xie W, Deng H (2017) Extraction, isolation and characterization of nanocrystalline cellulose from industrial kelp (Laminaria japonica) waste. Carbohydr Polym 173:353–359
30. Lu P, Hsieh YL (2010) Preparation and properties of cellulose nanocrystals: rods, spheres, and network. Carbohydr Polym 82(2):329–336
31. Lucas-Freile AD, Sancho-Querol S, Yáñez-Pacios AJ, Marín-Perales L, Martín-Martínez JM (2018) Blends of ethylene-co-vinyl acetate and poly (3-hydroxybutyrate) with adhesion property
32. Luo X, Benson RS, Kit KM, Dever M (2002) Kudzu fiber-reinforced polypropylene composite. J Appl Polym Sci 85(9):1961–1969
33. Luzi F, Fortunati E, Puglia D, Lavorgna M, Santulli C, Kenny JM, Torre L (2014) Optimized extraction of cellulose nanocrystals from pristine and carded hemp fibres. Ind Crops Prod 56:175–186
34. Mandal A, Chakrabarty D (2011) Isolation of nanocellulose from waste sugarcane bagasse (SCB) and its characterization. Carbohydr Polym 86(3):1291–1299
35. Marchessault RH, Liang CY (1962) The infrared spectra of crystalline polysaccharides. VIII. Xylans. J Polym Sci 59(168):357–378
36. Mensitieri G, Di Maio E, Buonocore GG, Nedi I, Oliviero M, Sansone L, Iannace S (2011) Processing and shelf life issues of selected food packaging materials and structures from renewable resources. Trends Food Sci Technol 22(2–3):72–80
37. Mondragon G, Fernandes S, Retegi A, Peña C, Algar I, Eceiza A, Arbelaiz A (2014) A common strategy to extracting cellulose nanoentities from different plants. Ind Crops Prod 55:140–148
38. Morán JI, Alvarez VA, Cyras VP, Vázquez A (2008) Extraction of cellulose and preparation of nanocellulose from sisal fibers. Cellulose 15(1):149–159
39. Mozdyniewicz DJ, Nieminen K, Kraft G, Sixta H (2016) Degradation of viscose fibers during acidic treatment. Cellulose 23(1):213–229
40. Nacos MK, Katapodis P, Pappas C, Daferera D, Tarantilis PA, Christakopoulos P, Polissiou M (2006) Kenaf xylan–a source of biologically active acidic oligosaccharides. Carbohydr Polym 66(1):126–134

41. Nelson ML, O'Connor RT (1964) Relation of certain infrared bands to cellulose crystallinity and crystal latticed type. Part I. Spectra of lattice types I, II, III and of amorphous cellulose. J Appl Polym Sci 8(3):1311–1324
42. Oh SY, Yoo DI, Shin Y, Seo G (2005) FTIR analysis of cellulose treated with sodium hydroxide and carbon dioxide. Carbohydr Res 340(3):417–428
43. Oksman K, Aitomäki Y, Mathew AP, Siqueira G, Zhou Q, Butylina S, Hooshmand S (2016) Review of the recent developments in cellulose nanocomposite processing. Compos Part A: Appl Sci Manufac 83:2–18
44. Petersen K, Nielsen PV, Bertelsen G, Lawther M, Olsen MB, Nilsson NH, Mortensen G (1999) Potential of biobased materials for food packaging. Trends Food Sci Technol 10(2):52–68
45. Rabemanolontsoa H, Saka S (2013) Comparative study on chemical composition of various biomass species. RSC Adv 3(12):3946–3956
46. Rodriguez-Perez S, Serrano A, Pantión AA, Alonso-Fariñas B (2018) Challenges of scaling-up PHA production from waste streams. A review. J Environ Manage 205:215–230
47. Segal LGJMA, Creely JJ, Jr M, Conrad CM (1959) An empirical method for estimating the degree of crystallinity of native cellulose using the X-ray diffractometer. Text Res J 29(10):786–794
48. Shi X, Jung KW, Kim DH, Ahn YT, Shin HS (2011) Direct fermentation of Laminaria japonica for biohydrogen production by anaerobic mixed cultures. Int J Hydrog Energy 36(10):5857–5864
49. Shimazaki Y, Miyazaki Y, Takezawa Y, Nogi M, Abe K, Ifuku S, Yano H (2007) Excellent thermal conductivity of transparent cellulose nanofiber/epoxy resin nanocomposites. Biomacromolecules 8(9):2976–2978
50. Shurtleff W, Aoyagi A (1977) The book of kudzu: a culinary & healing guide. Soyinfo Center
51. Stark NM (2016) Opportunities for cellulose nanomaterials in packaging films: A review and future trends. J Renew Mater 4(5):313–326
52. Sun XF, Xu F, Sun RC, Fowler P, Baird MS (2005) Characteristics of degraded cellulose obtained from steam-exploded wheat straw. Carbohydr Res 340(1):97–106
53. Sundarraj AA, Ranganathan TV (2018) A review on cellulose and its utilization from agro-industrial waste. Drug Invent Today 10(1):89–94
54. Sung SH, Chang Y, Han J (2017) Development of polylactic acid nanocomposite films reinforced with cellulose nanocrystals derived from coffee silverskin. Carbohydr Polym 169:495–503
55. Tanner RD, Hussain SS, Hamilton LA, Wolf FT (1979) Kudzu (Pueraria lobata): potential agricultural and industrial resource. Econ Bot 33(4):400–412
56. Tanner RD, Prokop A, Bajpai RK (1993) Removal of fiber from vines by solid state fermentation/enzymatic degradation: A comparison of flax and kudzu retting. Biotechnol Adv 11(3):635–643
57. Tarasov D, Leitch M, Fatehi P (2018) Lignin–carbohydrate complexes: properties, applications, analyses, and methods of extraction: a review. Biotechnol Biofuels 11(1):1–28

58. Uludag S, Loha V, Prokop A, Tanner RD (1996) The effect of fermentation (retting) time and harvest time on kudzu (Pueraria lobata) fiber strength. In Seventeenth Symposium on Biotechnology for Fuels and Chemicals (pp. 75–84). Humana Press, Totowa, NJ
59. Vanderfleet OM, Cranston ED (2021) Production routes to tailor the performance of cellulose nanocrystals. Nat Reviews Mater 6(2):124–144
60. Wang Y (2008) Cellulose fiber dissolution in sodium hydroxide solution at low temperature: Dissolution kinetics and solubility improvement. Georgia Institute of Technology
61. Wilke CR, Rosenberg S (1977) Analysis and evaluation of potential raw materials: chemical analysis of the kudzu plant. Quart. ERDA Report
62. Yahya MB, Lee HV, Abd Hamid SB (2015) Preparation of nanocellulose via transition metal salt-catalyzed hydrolysis pathway. BioResources 10(4):7627–7639
63. Yang H, Yan R, Chen H, Lee DH, Zheng C (2007) Characteristics of hemicellulose, cellulose and lignin pyrolysis. Fuel 86(12–13):1781–1788
64. Zhuang J, Li M, Pu Y, Ragauskas AJ, Yoo CG (2020) Observation of potential contaminants in processed biomass using fourier transform infrared spectroscopy. Appl Sci 10(12):4345

Figures

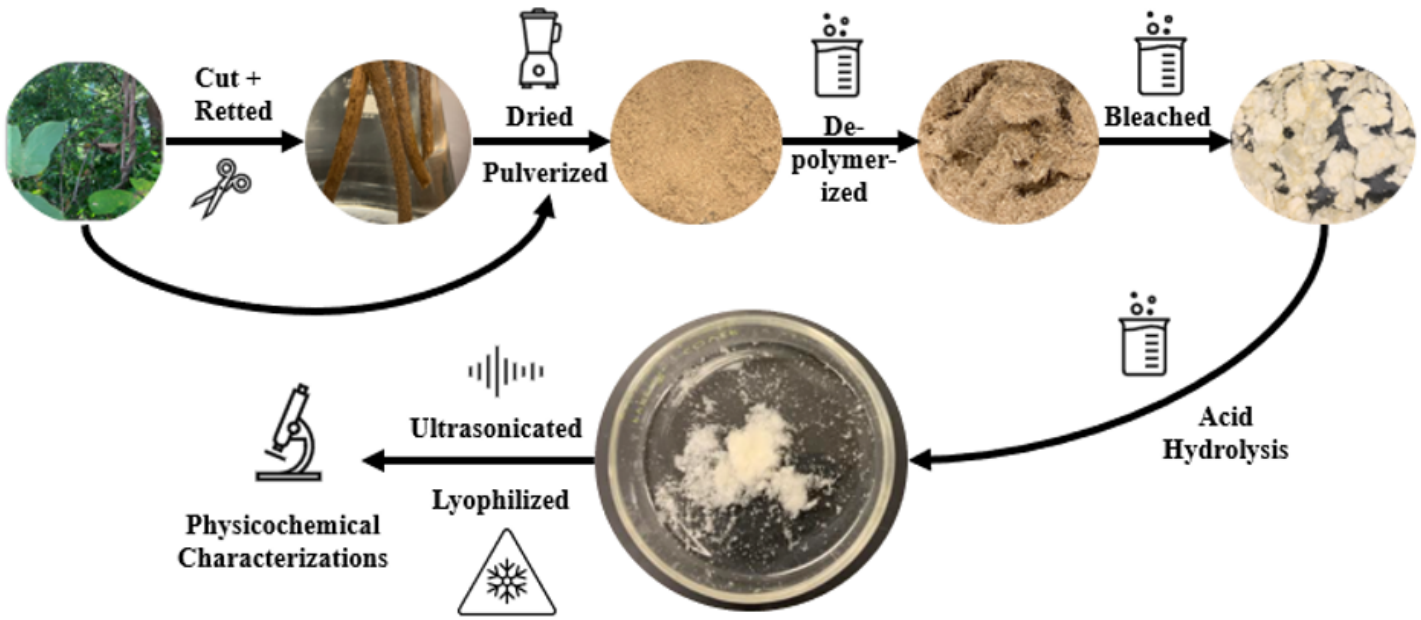

Figure 1

General overview of the widely accepted process used to extract CNCs.

Figure 2

TEM observation of the kudzu vine samples that underwent treatment. Rod-shaped nanocellulose particles were clearly distinguished in this nanoscale microscope image.

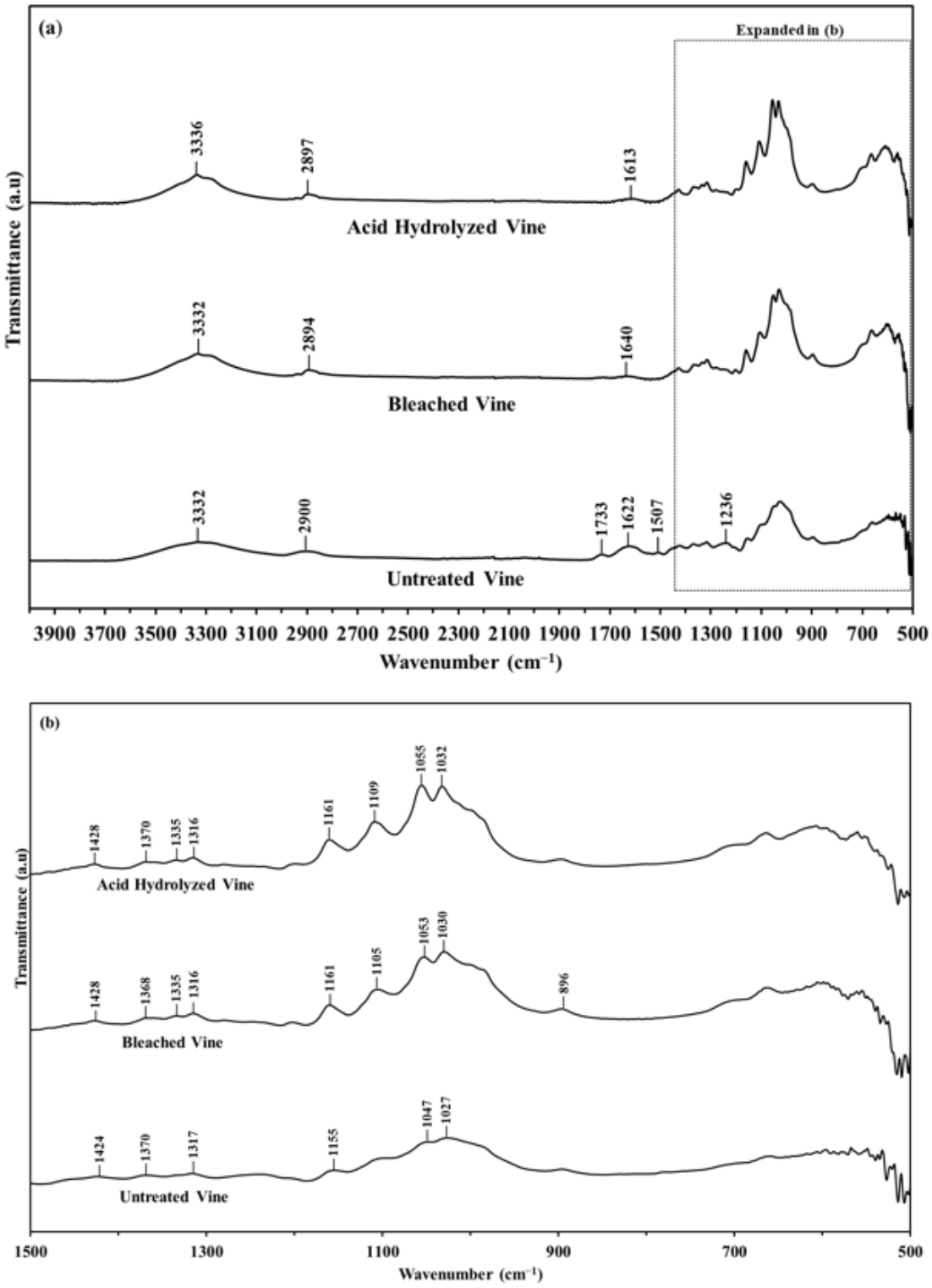

Figure 3

FTIR spectra of (a) the untreated vine, bleached vine, and acid hydrolyzed vine samples in the 4000-500 cm^{-1} region, and (b) expanded region between 1500-500 cm^{-1}.

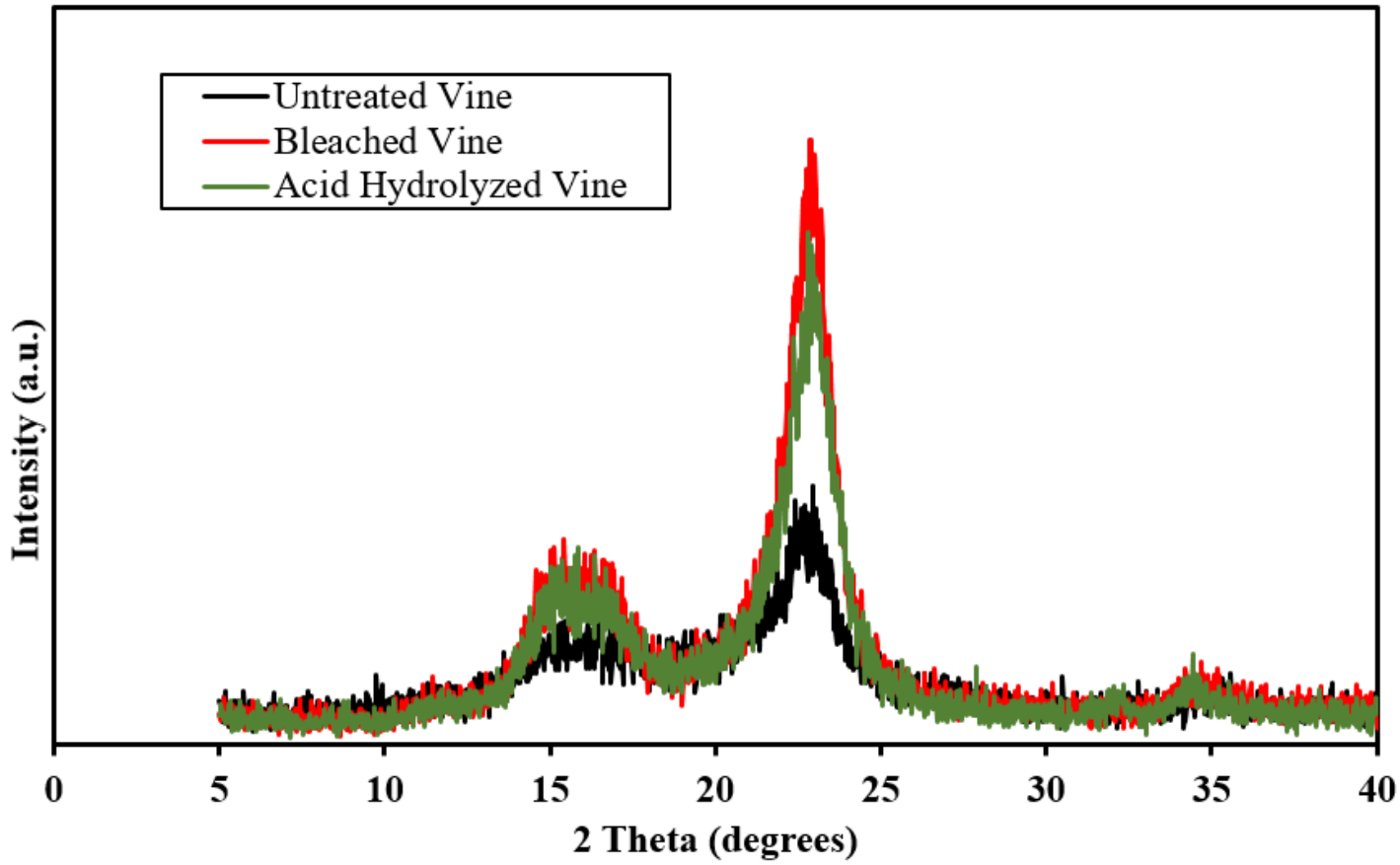

Figure 4

XRD patterns of the untreated, bleached, and acid hydrolyzed vine samples.

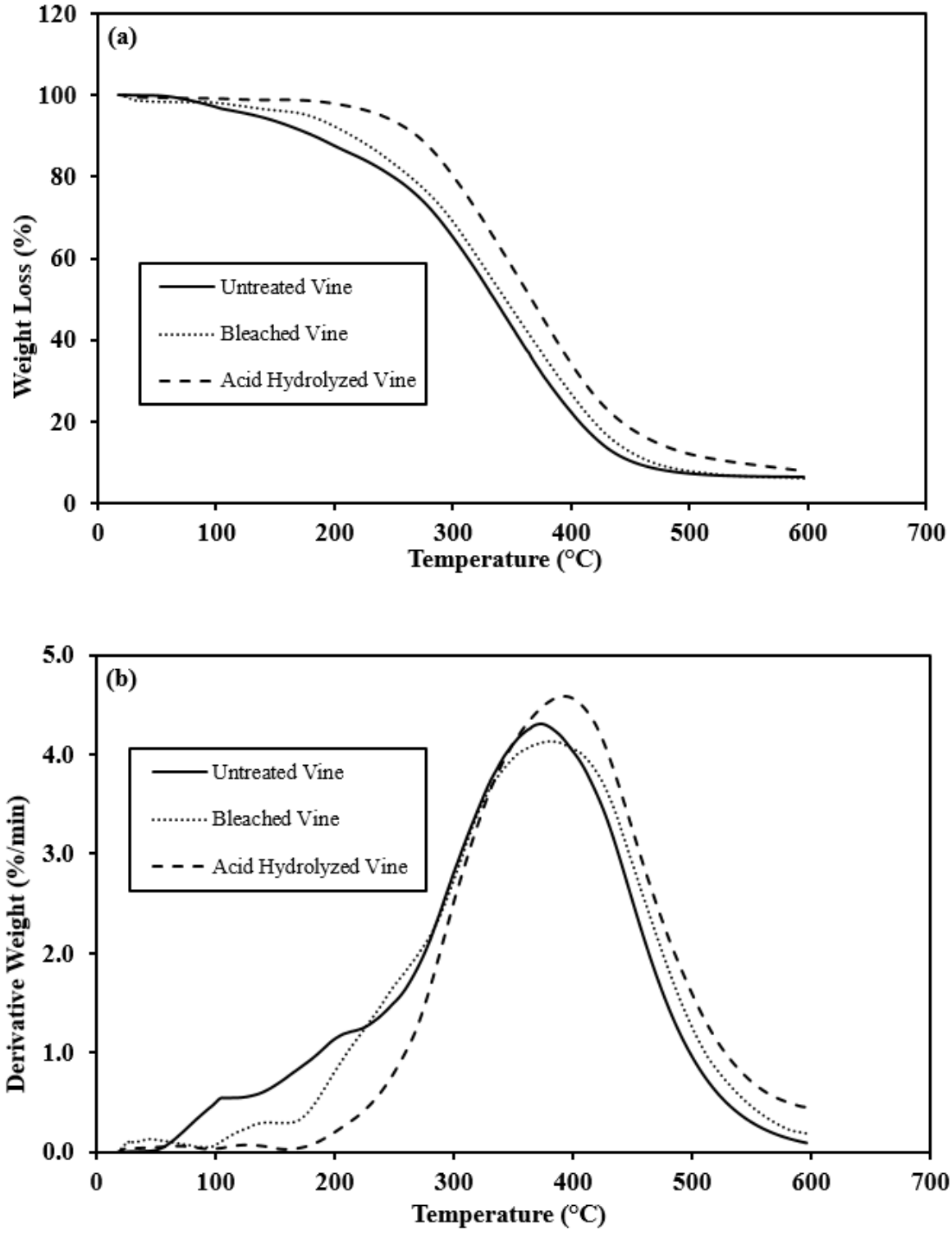

Figure 5

TGA (a) and DTG (b) curves of the kudzu vine after no treatment, bleaching, and acid hydrolysis.